Preprints of the 21st IFAC World Congress (Virtual)
Berlin, Germany, July 12-17, 2020

Nonlinear output feedback-feedforward control of tubular gasification reactors

Ulises Badillo-Hernández[1], Jesús Álvarez[2], Hugo A. Franco-de los Reyes[1] and Luis A. Álvarez-Icaza[1]
[1] Instituto de Ingeniería,
Universidad Nacional Autónoma de México, 04510 Cd. México, México
[2] Departamento de Ingeniería de Procesos e Hidráulica,
Universidad Autónoma Metropolitana-Iztapalapa, 09340 Cd. México, México

Abstract: The problem of robustly controlling open-loop bistable tubular gasification reactors about its ignition stable SS is addressed. To attenuate the effect of measured and unmeasured disturbances on closed-loop (CL) stability and caloric yield, the air feed flow must be adjusted on the basis of flow as well as inside point temperature measurements. The consideration of the problem as an efficient finite-dimensional model-based interlaced control-observer design yields a robust dynamic nonlinear (NL) output feedback (OF)-feedforward (FF) controller: (i) made by the combination of a passive NL state feedback (SF)-feedforward (FF) controller with a NL geometric (G) state estimator, and (ii) with CL stability conditions accompanied by gain tuning and sensor location guidelines. The approach is applied, through numerical simulations, to a 10-component 1-temperature and 2-flow stratified gasification reactor, finding that the nonlinear OF dynamic controller (made of 91 ODEs and 300 AEs) robustly stabilizes the reactor with preclusion of undesired SS ignition-to-extinction caused by solid feed disturbances.

Keywords: tubular gasification reactor, distributed parameter system; output feedback control; state estimator, disturbance rejection; sensor location.

1. INTRODUCTION

The industrial scale up of tubular exothermic moving solid bed gasification reactors, where solid biomass is efficiently disposed with energy generation, is limited by high effluent sensitivity composition with respect to feed composition, temperature and flowrate disturbances. These reactors have from 7 to 15 chemical species and from 1 or 2 temperatures, and their complex (with multiplicity and/or bifurcation)-nonlinear spatially distributed dynamics that modeled by a set of 12-to-20 nonlinear PDEs which have been solved, with finite-differences (FD) and computational fluid dynamics (CFD) methods, for the SS of interest and its start up (Di Blasi 2000; Rogel and Aguillon, 2006; Perez et al., 2012). The key multiplicity property has not been assessed with bifurcation-based numerical continuation on the basis of FD/CFD PDE-to-ODE discretization, perhaps due to the difficulty or even intractability of handling a high number of ill-conditioned nonlinear algebraic equations (Badillo-Hernández et al., 2019). The associated model-based control problem has not been addressed.

The estimation and control problem of fluidized bed coal gasification reactors, of a less distributed nature and easier to model in comparison to biomass moving bed reactors, have been studied on the basis of a PDE-to- 25 ODE discrete model with a diversity of conventional (multivariable PI, model predictive control) and advanced (H_∞, sliding mode, genetic algorithms, Kalman filter-based) techniques for the well known ALSTOM benchmark example (Dixon and Pike, 2006). The extension of these techniques to the biomass moving bed gasification reactor case, with considerably more model equations, is by no means a trivial task.

The control of tubular reactors with complex nonlinear dynamics has been addressed with early (PDE-to-ODE model discretization followed by control design) and late lumping (PDE model-based design with discretization at implementation) approaches, the state of the art can be seen elsewhere (Beniich et al., 2017; Meurer and Zeitz, 2008), and here it suffices to say that: (i) only reactors with few (two and three)-state profiles have been considered, (ii) late lumping focuses on formal convergence proofs at the const of more complex mathematics, (ii) the direct application of early and late lumping approaches to many-species reactors, like the gasification reactors, lead to discrete control systems, made by a large number of (possibly ill-conditioned) nonlinear ordinary and algebraic equations with on-line computational load that is an obstacle for industrial applicability.

The preceding consideration motivate the present efficient model-based (Badillo-Hernández et al., 2019) control design study on biomass moving bed gasification reactors, with efficiency meaning: robust (with respect to PDE-to-ODE order) and quantitative (up to kinetic-transport parameter uncertainty) description of the complex (with multiplicity and bifurcation) global-nonlinear PDE dynamics of the open-loop (OL) gasification reactor.

Our points of departure are: (i) the efficient model-based stabilizing nonlinear (NL) state feedback (SF) passive control of a two-state tubular reactor (Najera et al, 2016), and (ii) the geometric nonlinear state estimator for one (Fernandez et al., 2012) and many (Porru et al., 2013)-state staged distillation columns with spatial structure similar to the one of FD-based tubular reactor models (Badillo-Hernández et al., 2017).

The problem is solved by designing an efficient model-based robustly stabilizing passive NL SF controller implemented with a NL geometric state estimator (GE), including: (i) systematic and simple construction-tuning procedure, (ii) CL robust state stability conditions coupled with sensor location

and gain tuning, and (iii) considerably less on-line computational load with respect to previous early and late-lumping approaches.

The proposed approach is illustrated through numerical simulation with a representative stratified bistable reactor example with model calibrated against experimental data (Badillo-Hernández, et al., 2019), with 13 state profiles (2-flows, 1-temperature, and 10-compositions), and undesirable OL SS ignition-to-extinction transition by feed disturbance.

2. CONTROL PROBLEM

Consider the stratified tubular gasification reactor of length L, transversal area A and total metal mass m_w shown in Fig. 1, where solid (s) and gas (g) streams (fed at the top) are transformed, through a multicomponent (pyrolysis, combustion and reduction) reaction network (Di Blasi, 2000) coupled with mass and heat convective-dispersive transport and wall heat losses, into an effluent (bottom) stream with syngas, char and ashes.

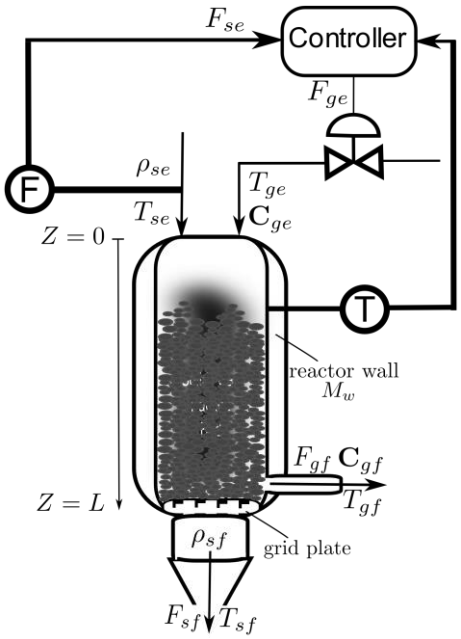

Fig. 1. Stratified gasification reactor and control scheme.

Without restricting the approach, in this study we will consider that the OF-FF controller will be driven by three input measurements: the solid feed flow (F_{se}), gas (T_{ge}) and solid (T_{se}) feed temperatures, and one output temperature measurement at a suitable axial location (to be precised).

From standard assumptions on (quasistatic –QSS- gas dynamics and large gas-solid heat exchange) (Hlavacek, 1970), the reactor dynamics are described by the following set of nonlinear PDEs (Badillo-Hernandez et al., 2019):

$$0 = -\partial_z\left[\left(F_g/A_R\right)\right] + \boldsymbol{m}_g^T\boldsymbol{R}(\boldsymbol{C},T), \quad 0 < z \le L, \ t > 0 \tag{1a}$$

$$0 = -\partial_z(F_s/A_R) - \boldsymbol{s}_C^T\boldsymbol{R}(\boldsymbol{C},T), \quad \boldsymbol{C} = \left[\boldsymbol{C}_s^T, \boldsymbol{C}_g^T\right]^T \tag{1b}$$

$$0 = -\partial_z\left[\left(F_g/\rho_g(T)A_R\right)\boldsymbol{C}_g\right] + \boldsymbol{S}_g^T\boldsymbol{R}(\boldsymbol{C},T) \tag{1c}$$

$$\partial_t\boldsymbol{C}_s = -\partial_z([F_s/\rho_s A_R]\boldsymbol{C}_s) + \boldsymbol{S}_s^T\boldsymbol{R}(\boldsymbol{C},T) \tag{1d}$$

$$\partial_t T = H_s^{-1}(\boldsymbol{C}_s)\{\partial_z[K(T)\partial_z T] - V_h(\boldsymbol{v},\boldsymbol{C},T)\partial_z T - h_w(T)(T-T_a) + \boldsymbol{\Delta H}^T\boldsymbol{R}(\boldsymbol{C},T)\} \tag{1e}$$

with boundary and initial conditions

$$z = 0\text{: } (F_g, F_s, \boldsymbol{C}_g, \boldsymbol{C}_s)(0,t) = (F_{ge}, F_{se}, \boldsymbol{C}_{ge}, \boldsymbol{C}_{se}), \quad K(T)\partial_z T = v_h(\boldsymbol{v},\boldsymbol{C},T)(T-T_e) \tag{1f}$$

$$z = L\text{: } K(T)\partial_z T = h_\gamma(T)(T-T_a) \tag{1g}$$

$$t = 0\text{: } (\boldsymbol{C}_s, T)(z,0) = (\boldsymbol{C}_{so}, T_o)(z) \tag{1h}$$

• *Dynamic ($\boldsymbol{\chi}$) and quasistatic ($\boldsymbol{\eta}$) state profiles*

$$\boldsymbol{\chi} = (\boldsymbol{C}_s, T)^T, \qquad \boldsymbol{\eta} = (\boldsymbol{C}_g, F_g, F_s)^T \tag{2a-b}$$

• *Measured ($\boldsymbol{d}$) and unmeasured ($\boldsymbol{\varrho}$) disturbances*

$$\boldsymbol{d} = (F_{se}, T_{ge}, T_{se}), \qquad \boldsymbol{\varrho} = (\boldsymbol{C}_{ge}^T, \boldsymbol{C}_{se}^T) \tag{3a-b}$$

• *Control input (u) and output measurement (y)*

$$u = F_{ge}, \qquad y = T(z_l,t), \qquad z_l \in \mathcal{Z} = (0,L) \tag{4a-b}$$

where z is the axial position, t is the time, $\boldsymbol{C}_s$ is the n_s-concentration vector, T is the temperature, $\boldsymbol{C}_g$ is the n_g-concentration vector, F_g (or F_s) is the mass flow of gas (or solid) phase, T_a is the ambient temperature, F_{ge} (or F_{se}) is the convective gas (or solid) feed rate with concentration $\boldsymbol{C}_{ge}$ (or $\boldsymbol{C}_{se}$) and temperature T_{ge} (or T_{se}).

The vector $\boldsymbol{R}$ contains the n_r reaction rates, $\boldsymbol{S}_g$ (or $\boldsymbol{S}_s$) is the stoichiometric matrix of gas (or solid) phase, $\boldsymbol{s}_C$ is the vector of stoichiometric coefficients of char and (-$\boldsymbol{\Delta H}$) is made of the n_r heats of reaction. K is the effective heat conductivity that includes dispersion and radiation, V_h (or H_s) is the convective heat flux (or capacity), and h_w (or h_γ) is the wall (or grid) heat exchange function.

In compact form, the PDE model (1) is written as:

$$\partial_t\boldsymbol{\chi} = \boldsymbol{\mathcal{F}}_\chi(\boldsymbol{\chi},\boldsymbol{\varrho},\boldsymbol{d},u), \ \boldsymbol{\mathcal{B}}(\boldsymbol{\chi},\boldsymbol{\varrho},\boldsymbol{d}) = \boldsymbol{0}, \ \boldsymbol{\chi}(0) = \boldsymbol{\chi}_o \tag{5a-b}$$

$$\boldsymbol{\eta} = \boldsymbol{\mathcal{G}}(\boldsymbol{\chi},\boldsymbol{\varrho},\boldsymbol{d},u), \qquad \boldsymbol{\pi} = (\boldsymbol{\chi}^T, \boldsymbol{\eta}^T)^T \tag{5c-d}$$

$$y = \boldsymbol{c}_y\boldsymbol{\chi}(z_l,t) = T(z_l,t), \ \boldsymbol{c}_y = (0,0,\dots,0,1), \ z_l \in \mathcal{Z} \tag{5e}$$

where (RHS: right hand side)

$$\boldsymbol{\chi}(t) = (\boldsymbol{C}_s, T)^T, \qquad \boldsymbol{\eta} = (\boldsymbol{C}_g, F_g, F_s)^T \tag{6a-b}$$

$$\boldsymbol{d} = (F_{se}, T_{ge}, T_{se}), \quad \boldsymbol{\varrho} = (\boldsymbol{C}_{ge}^T, \boldsymbol{C}_{se}^T), \quad u = F_{ge} \tag{6c-d}$$

$$\dim\boldsymbol{\chi} = n_\chi = n_s + 1, \quad \dim\boldsymbol{\eta} = n_\eta = n_g + 2 \tag{6e-f}$$

$$\dim\boldsymbol{C}_s = n_s, \qquad \dim\boldsymbol{C}_g = n_g \tag{6g-h}$$

$\boldsymbol{\mathcal{G}}$: solution for $\boldsymbol{\eta}$ of (1a-c) (6i)

$\boldsymbol{\mathcal{F}}_\chi$: RHS of (1d-e) with $\boldsymbol{\eta}$ substituted by (6i) (6j)

$\boldsymbol{\mathcal{B}}$: boundary conditions of (1d-e) substituted by (6i) (6k)

$\boldsymbol{\chi}$ (or $\boldsymbol{\eta}$) is the dynamic (or quasistatic) state, $\boldsymbol{d}$ (or y) is the measured input (or point output), $\boldsymbol{\varrho}$ is the unmeasured input, and u is the domain control input.

The PDE model has the open-loop (OL) steady-state (SS) set

$$\Sigma = \{\overline{\boldsymbol{\chi}}_E, \overline{\boldsymbol{\chi}}_U, \overline{\boldsymbol{\chi}}_I\} \tag{7}$$

with stable desired ignition (or undesired extinction) SS $\overline{\boldsymbol{\chi}}_I$ (or $\overline{\boldsymbol{\chi}}_E$), and unstable saddle $\overline{\boldsymbol{\chi}}_U$ (between $\overline{\boldsymbol{\chi}}_I$ and $\overline{\boldsymbol{\chi}}_E$) which determines the size of the basin of attraction of $\overline{\boldsymbol{\chi}}_I$. The fact that feed disturbances ($\boldsymbol{d}$) (3b) can cause undesired ignition-to-extinction OL SS transition (Badillo-Hernandez et al. 2019) motivates its preclusion through measurement-driven control.

2.1 Output feedback control problem

Our problem consists in designing an output dynamic feedback (OF)-feedforward (FF) controller (depicted in Figure 1), which, driven by the measured input-output signal pair ($\boldsymbol{d}, y$) (3a,4b), yields a robustly (R)-stable closed loop (CL) operation about the nominal ignition SS $\overline{\boldsymbol{\chi}}_I$ (7) with admissible state profile ($\boldsymbol{\pi}$) variability in spite of persistent bounded

disturbance $(\boldsymbol{\varrho}, \boldsymbol{d})$ (3a-b) that can induce OL extinction. An adequate compromise between state profile variability, control effort, robustness and on-line computational load (which reflects number of equations, and their ill-conditioning) must be attained.

A biomass downdraft stratified gasification bistable (Badillo-Hernandez et al. 2019) tubular reactor (Manurung and Beenackers, 1993) (Figure 1) will be considered as example, with: (i) $n_r = 10$ reactions and $n_g = 8$ (or $n_s = 2$) gas (or solid) species

$$B_s = \{B, C\}, B_g = \{O_2, H_2, CO, CO_2, H_2O, CH_4, Tars, N_2\} \quad (8)$$

(ii) kinetic-transport (KT) functions (Di Blasi, 2000) with parameters calibrated (Badillo-Hernandez et al. 2019) against experimental data (Manurung & Beenackers,1993), and (iii) temperature profile triplet (Fig. 2) of the SS set (7) computed with a (uniform 200-node) FD PDE numerical solver.

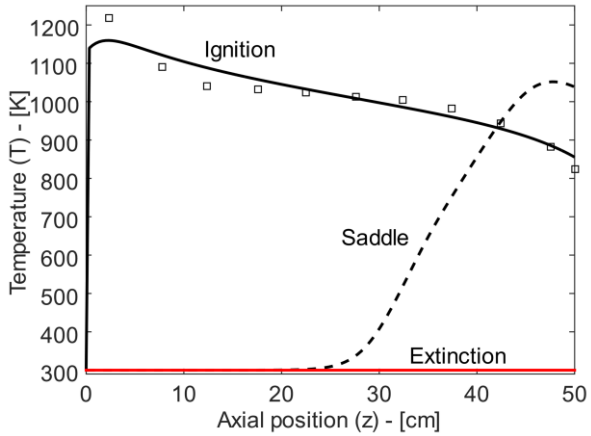

Fig. 2. SS temperature profiles of the bistable reactor (7). □: experimental data (Manurung & Beenackers,1993).

3. FINITE-DIMENSIONAL MODEL

The application to the PDE model (1,6) of the efficient FD-based *convergent* (LeVeque, 2007) spatial discretization (with first-order backwards for convection and second-order centered differences for dispersion) for heterogeneous tubular reactors (Badillo-Hernandez et al, 2019) leads to the low-order *N-stage differential-algebraic (DAE) model*

$$\dot{\boldsymbol{x}} = \boldsymbol{f}(\boldsymbol{x}, \boldsymbol{\varrho}, \boldsymbol{d}, u), \quad \boldsymbol{x}(0) = \boldsymbol{x}_o \quad (9a)$$
$$\boldsymbol{\zeta} = \boldsymbol{g}(\boldsymbol{x}, \boldsymbol{\varrho}, \boldsymbol{d}, u), \quad z \in Z = [0, L] \quad (9b)$$
$$\boldsymbol{\chi}_N(z,t) = \boldsymbol{C}_x^N(z)\boldsymbol{x}(t), \quad (9c)$$
$$\boldsymbol{\eta}_N(z,t) = \boldsymbol{C}_\zeta^N(z)\boldsymbol{\zeta}(t), \quad (9d)$$
$$y = \boldsymbol{c}_l \boldsymbol{x} = T_l, \quad \boldsymbol{c}_l = \boldsymbol{c}_y \boldsymbol{C}_x^N(z_l), \quad l \in [1, N] \quad (9e\text{-}f)$$

where

$$\boldsymbol{x} = (\boldsymbol{x}_1^T, \dots, \boldsymbol{x}_N^T)^T, \quad \boldsymbol{x}_i = (\boldsymbol{C}_{si}^T, T_i)^T, \quad \dim \boldsymbol{x} = n_\chi N := n$$
$$\boldsymbol{\zeta} = (\boldsymbol{\zeta}_1^T, \dots, \boldsymbol{\zeta}_N^T)^T, \quad \boldsymbol{\zeta}_i = \left(\boldsymbol{C}_{gi}^T, Q_{gi}, Q_{si}\right)^T, \dim \boldsymbol{\zeta} = n_\eta N := n_\zeta$$
$$N = \kappa_q\left(N_{pde}, \tilde{\boldsymbol{p}}\right) < N_{pde} \in [200{,}500] \quad (10)$$

where $\boldsymbol{x}$ (or $\boldsymbol{\zeta}$) is the dynamic (or quasi-static) state, $\boldsymbol{C}_x^N$ [or $\boldsymbol{C}_\zeta^N$] is the interpolation matrix that yields the approximation $\boldsymbol{\chi}_N$ (or $\boldsymbol{\eta}_N$) of the state profile $\boldsymbol{\chi}$ (or $\boldsymbol{\eta}$) from $\boldsymbol{x}$ (or $\boldsymbol{\zeta}$), u is the control input, $\boldsymbol{d}$ (or $\boldsymbol{\varrho}$) is the measured (or unmeasured) input disturbance, y is the temperature measurement at the l-th sensor location.

The efficient stage number N, determined through algorithm (10) (Badillo-Hernandez et al, 2019), is the smallest integer which ensures that the N-stage model (9) robustly (with respect to single-stage number change) and quantitatively (up to KT parameter uncertainty $\tilde{\boldsymbol{p}}$) describes, the global-nonlinear PDE dynamics (5) approximated by a standard N_{pde}-node FD numerical solver (9).

The application of the efficient stage algorithm (8) with $N_{pde} = 200$ (Di Blasi, 2000) to example (8) yields the *efficient stage number* (Badillo-Hernandez et al., 2019):

$$N = 30 < N_{pde} = 200 \quad (11)$$

with OL SS set ($\Leftrightarrows$: topologically equivalent)

$$S = \{\bar{\boldsymbol{x}}_E, \bar{\boldsymbol{x}}_U, \bar{\boldsymbol{x}}_I\} \Leftrightarrows \Sigma, \quad \Sigma{:}(7), \quad \bar{\boldsymbol{x}}_U\text{: unstable saddle SS} \quad (12)$$
$$\bar{\boldsymbol{x}}_I \text{ (or } \bar{\boldsymbol{x}}_E\text{): stable desired (or undesired) SS}$$
$$\bar{\boldsymbol{x}}_U\text{: boundary of the bassins of attraction of } \bar{\boldsymbol{x}}_I \text{ and } \bar{\boldsymbol{x}}_E$$

In Fig. 3 (bottom panel) is presented the undesired ignition ($\bar{\boldsymbol{x}}_I$)-to-extinction ($\bar{\boldsymbol{x}}_E$) SS OL transient (with duration of 51 mins) induced by a squared pulse-like disturbance increase of solid feed flow rate (top panel). The settling time of the local dynamics is (λ_r:logaritmic rate of change)

$$t_s = 8 \text{ min} \Rightarrow \lambda_r = 4/t_s = 1.2\ min^{-1} \quad (13)$$

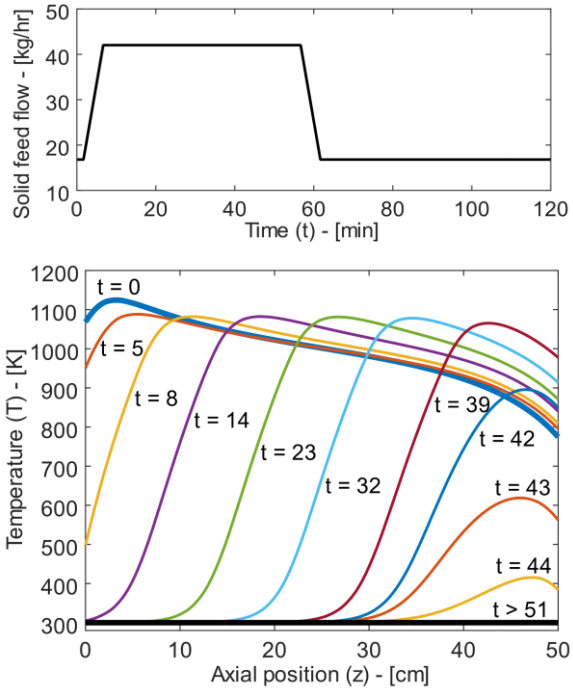

Fig. 3. Open-loop SS ignition (blue curve)-to-extinction (black curve) temperature profile transient (bottom panel) induced by a solid feed flow squared pulse disturbance (top panel).

Thus, the OF control task is to maintain the reactor at the prescribed nominal SS $\bar{\boldsymbol{x}}_I$, in spite of admissible bounded disturbances $\tilde{\boldsymbol{d}}(t)$.

4. STATE FEEDBACK-FEEDFORWARD CONTROL

Here, the NL SF-FF control problem is addressed by extending to the many-profile gasification reactor case the NLSF component of the NLOF controller of a two-profile single-

reaction staged reactor (Najera et al., 2016) and a multicomponent distillation column (Porru et al., 2013).

For this aim, let us write the N-stage model (9) in the partitioned form:

$$\dot{x}_c = f_c(\boldsymbol{x}, \boldsymbol{\varrho}, \boldsymbol{d}, u), \quad x_c(0) = x_{co}, \quad z \in Z = [0, L] \tag{14a}$$
$$\dot{\boldsymbol{x}}_z = \boldsymbol{f}_z(\boldsymbol{x}, \boldsymbol{\varrho}, \boldsymbol{d}, u), \quad \boldsymbol{x}_z(0) = \boldsymbol{x}_{zo} \tag{14b}$$
$$\boldsymbol{\zeta} = \boldsymbol{g}(\boldsymbol{x}, \boldsymbol{\varrho}, \boldsymbol{d}, u), \quad j = 1, \dots, m-1 \tag{14c}$$
$$y = \boldsymbol{c}_l \boldsymbol{x} = x_c = T_l, \qquad l \in [1, N] \tag{14d}$$
$$\boldsymbol{\chi}_N(z,t) = \boldsymbol{C}_x^N(z)\boldsymbol{x}(t), \quad \boldsymbol{\eta}_N(z,t) = \boldsymbol{C}_\zeta^N(z)\boldsymbol{\zeta}(t) \tag{14e-f}$$

where

$$\boldsymbol{x} = \boldsymbol{I_p}(x_c, \boldsymbol{x}_z^T)^T, \qquad \dim \boldsymbol{x}_z = n - 1$$

y is the output measurement of the temperature state $x_c = T_l$ at l-th location z_l (9e-f) to be (directly) regulated by the SF-FF controller and $\boldsymbol{I_p}$ is the state permutation matrix.

4.1 Passive SF-FF control

The task is to adjust the air feed flow u to regulate the temperature measurement y about the setpoint $\bar{y}$.

The enforcement of the prescribed linear output regulation dynamics (where k is an adjustable gain)

$$\dot{e}_y = -k e_y, \quad e_y = y - \bar{y} \tag{15a-b}$$

on (14) yields the NLSF controller in implicit form

$$f_c(\boldsymbol{x}, \boldsymbol{\varrho}, \boldsymbol{d}, u) + k(x_c - \bar{y}) = 0 \tag{16}$$

and the unique solution for u of this algebraic equation yields the *SF-FF temperature controller*

$$u = \mu_y(\boldsymbol{x}, \boldsymbol{\varrho}, \boldsymbol{d}, \bar{y}) \tag{17}$$

whose application to (14) yields the CL dynamics

$$\dot{x}_c = k(x_c - \bar{y}), \qquad x_c(0) = x_{co}; \quad y = x_c \tag{18a-b}$$
$$\dot{\boldsymbol{x}}_z = \boldsymbol{\mathit{f}}_z(\boldsymbol{x}, \boldsymbol{\varrho}, \boldsymbol{d}, \bar{y}), \quad \boldsymbol{x}_z(0) = \boldsymbol{x}_{zo} \tag{18c}$$
$$\boldsymbol{\zeta} = \boldsymbol{\mathit{g}}(\boldsymbol{x}, \boldsymbol{\varrho}, \boldsymbol{d}, \bar{y}) \tag{18d}$$
$$\boldsymbol{\chi}_N(z,t) = \boldsymbol{C}_x^N(z)\boldsymbol{x}(t), \quad \boldsymbol{\eta}_N(z,t) = \boldsymbol{C}_\zeta^N(z)\boldsymbol{\zeta}(t) \tag{18e-f}$$

where

$$\boldsymbol{\mathit{f}}_z(\boldsymbol{x}, \boldsymbol{\varrho}, \boldsymbol{d}, \bar{y}) = \boldsymbol{f}_z\big[\boldsymbol{x}, \boldsymbol{\varrho}, \boldsymbol{d}, \mu_y(\boldsymbol{x}, \boldsymbol{\varrho}, \boldsymbol{d}, \bar{y})\big]$$
$$\boldsymbol{\mathit{g}}(\boldsymbol{x}, \boldsymbol{\varrho}, \boldsymbol{d}, \bar{y}) = \boldsymbol{g}\big[\boldsymbol{x}, \boldsymbol{\varrho}, \boldsymbol{d}, \mu_y(\boldsymbol{x}, \boldsymbol{\varrho}, \boldsymbol{d}, \bar{y})\big]$$

The setting of $y = \bar{y}$ in the CL dynamics (18) yields the sensor location (z_l)-dependent (n-1)-dimensional *zero dynamics* (ZD) (19) and their associated NL SF *control* (20)

$$\dot{\boldsymbol{x}}_z^* = \boldsymbol{\mathit{f}}_z^*(\boldsymbol{x}_z^*, \boldsymbol{\varrho}, \boldsymbol{d}, \bar{y}), \ \boldsymbol{x}_z^*(0) = \boldsymbol{x}_{zo}^*; \quad x_c^* = \bar{y} \tag{19a-b}$$
$$\boldsymbol{\zeta}^* = \boldsymbol{\mathit{g}}^*(\boldsymbol{x}_z^*, \boldsymbol{\varrho}, \boldsymbol{d}, \bar{y}), \qquad \boldsymbol{x}^* = \boldsymbol{I_p}(x_c^*, \boldsymbol{x}_z^{*T})^T \tag{19c}$$
$$\boldsymbol{\chi}_N^*(z,t) = \boldsymbol{C}_x^N(z)\boldsymbol{x}^*(t), \quad \boldsymbol{\eta}_N^*(z,t) = \boldsymbol{C}_\zeta^N(z)\boldsymbol{\zeta}^*(t) \tag{19d-e}$$
$$u = \mu_z(\boldsymbol{x}_z^*, \boldsymbol{\varrho}, \boldsymbol{d}, \bar{y}) \tag{20}$$

where

$$\boldsymbol{\mathit{f}}_z^*(\boldsymbol{x}_z^*, \boldsymbol{\varrho}, \boldsymbol{d}, \bar{y}) = \boldsymbol{f}_z[\bar{y}, \boldsymbol{x}_z^*, \boldsymbol{\varrho}, \boldsymbol{d}, \mu_z(\boldsymbol{x}_z^*, \boldsymbol{\varrho}, \boldsymbol{d}, \bar{y})]$$
$$\boldsymbol{\mathit{g}}^*(\boldsymbol{x}_z^*, \boldsymbol{\varrho}, \boldsymbol{d}, \bar{y}) = \boldsymbol{g}[\bar{y}, \boldsymbol{x}_z^*, \boldsymbol{\varrho}, \boldsymbol{d}, \mu_z(\boldsymbol{x}_z^*, \boldsymbol{\varrho}, \boldsymbol{d}, \bar{y})]$$

(20) is the solution for u of the algebraic equation ($>_r$: robustly -sufficiently- larger than zero)

$$f_c(\bar{y}, \boldsymbol{x}_e^*, \boldsymbol{x}_z^*, \boldsymbol{\varrho}, \boldsymbol{d}, u) = 0, \quad \partial_u f_c >_r 0 \tag{21a-b}$$

and the corresponding *passivity* solvability conditions are given by

$$rd(u, y) = 1 \leftrightarrow f_c\text{: } u\text{-invertible}, \quad ZD \text{ (19) R-stable} \tag{22a,b}$$

The sensor location (z_l) is the one for which the ZD (19) has the best compromise between robustness, speed, and control effort.

5. OUTPUT FEEDBACK-FEEDFORWARD CONTROL

The efficient N_o-stage model-based NL OF-FF controller is constructed by combining the NL SF-FF controller (17) with the geometric estimator (GE) [Fernandez et. al., 2012] closed-loop counterpart (23a-d) of the open-loop one for the reactor example (Badillo-Hernandez et al., 2017):

$$\dot{\hat{x}}_c = -k(\hat{x}_c - \bar{y}) + 2\zeta\omega(y - \hat{x}_c) + \hat{\imath}, \ \hat{x}_c(0) = \hat{x}_{co} \tag{23a}$$
$$\dot{\hat{\boldsymbol{x}}}_z = \boldsymbol{\mathit{f}}_z(\hat{\boldsymbol{x}}, \bar{\boldsymbol{\varrho}}, \boldsymbol{d}, \bar{y}), \quad \hat{\boldsymbol{x}}_z(0) = \hat{\boldsymbol{x}}_{zo} \tag{23b}$$
$$\dot{\hat{\imath}} = \omega^2(y - \hat{x}_c), \qquad \hat{\imath}(0) = \hat{\imath}_o \tag{23c}$$
$$\hat{\boldsymbol{\zeta}} = \boldsymbol{\mathit{g}}(\hat{\boldsymbol{x}}, \bar{\boldsymbol{\varrho}}, \boldsymbol{d}, \bar{y}), \qquad l \in [1, N] \tag{23d-e}$$
$$u = \mu_y(\hat{\boldsymbol{x}}, \bar{\boldsymbol{\varrho}}, \boldsymbol{d}, \bar{y}), \qquad \hat{\boldsymbol{x}} = \boldsymbol{I}_p(\hat{x}_c, \hat{\boldsymbol{x}}_z^T)^T \tag{23f-g}$$
$$\hat{\boldsymbol{\chi}}(z,t) = \boldsymbol{C}_x^N(z)\hat{\boldsymbol{x}}(t), \quad \hat{\boldsymbol{\eta}}(z,t) = \boldsymbol{C}_\zeta^N(z)\hat{\boldsymbol{\zeta}}(t) \tag{23h-i}$$

where

$$\hat{\boldsymbol{x}}_E = (\hat{\boldsymbol{x}}^T, \hat{\imath}^T)^T, \ \dim \hat{\boldsymbol{x}}_E = n_e = n + 1$$

The closed-loop (CL) R-convergent N-stage state estimator (23a-d) is constructed by applying the GE approach with detectability index equal to one (Alvarez and Fernandez et. al., 2009; Fernandez et. al., 2012) to the CL efficient N-stage reactor model (18).

5.1 Closed loop stability

The SS $\bar{\boldsymbol{x}}$ of the nonlinear system (L: Lipschitz)

$$\dot{\boldsymbol{x}} = \boldsymbol{f}[\boldsymbol{x}, \boldsymbol{\varrho}(t), \boldsymbol{d}(t)], \quad \boldsymbol{x}(0) = \boldsymbol{x}_o, \ \boldsymbol{g}(\bar{\boldsymbol{x}}, \bar{\boldsymbol{\varrho}}, \bar{\boldsymbol{d}}) = \boldsymbol{0} \tag{24a}$$
$$|\boldsymbol{\varrho}(t) - \bar{\boldsymbol{\varrho}}| \le \varepsilon_\varrho, |\boldsymbol{d}(t) - \bar{\boldsymbol{d}}| \le \varepsilon_d, \ \boldsymbol{g}\text{: L-bounded} \tag{24b}$$

is robustly stable -with respect to admissible bounded inputs $\boldsymbol{\varrho}$ and $\boldsymbol{d}$- if $\bar{\boldsymbol{x}}$ is exponentially ultimately bounded [also called input-to state stable (ISS) (Sontag, 2000)] (Khalil, 2002) if the state motions $\boldsymbol{x}(t)$ of (24) are bounded as

$$|\boldsymbol{x}(t) - \bar{\boldsymbol{x}}| \le a_x |\boldsymbol{x}_o| e^{-\lambda_z t} + b_d \varepsilon_d + b_\varrho \varepsilon_\varrho, \lambda_z, b_d, b_\varrho > 0 \tag{25}$$

The CL dynamics (18) is the interconnection

$$\dot{\boldsymbol{x}} = \boldsymbol{\mathit{f}}(\boldsymbol{x}) + \tilde{\boldsymbol{\mathit{f}}}(\boldsymbol{x}, \tilde{\boldsymbol{x}}_E, \tilde{\boldsymbol{d}}_a), \boldsymbol{x}(0) = \boldsymbol{x}_o, \tilde{\boldsymbol{\mathit{f}}}(\bar{\boldsymbol{x}}, \boldsymbol{0}, \boldsymbol{0}) = \boldsymbol{0} \tag{26a}$$
$$\dot{\tilde{\boldsymbol{x}}}_E = \boldsymbol{\mathit{f}}_E(\tilde{\boldsymbol{x}}_E) + \tilde{\boldsymbol{\mathit{f}}}_E(\boldsymbol{x}, \tilde{\boldsymbol{x}}_E, \tilde{\boldsymbol{d}}_a), \tilde{\boldsymbol{x}}_E(0) = \tilde{\boldsymbol{x}}_{Eo}, \tilde{\boldsymbol{\mathit{f}}}_E(\bar{\boldsymbol{x}}, \boldsymbol{0}, \boldsymbol{0}) = \boldsymbol{0} \tag{26b}$$
$$\tilde{\boldsymbol{d}}_a = \big(\tilde{\boldsymbol{\varrho}}^T, \tilde{\boldsymbol{d}}^T\big)^T, \ |\tilde{\boldsymbol{d}}_a(t)| \le \varepsilon_{d_a}, \ \tilde{\boldsymbol{\mathit{f}}}, \tilde{\boldsymbol{\mathit{f}}}_E\text{: L-bounded} \tag{26c}$$

of two by-construction individually robustly stable (24) subsystems: (26a) CL state dynamics (18) with NLSF disturbance and estimation errors (26c), and (ii) CL state estimation error dynamics: (19a-d) minus (18).

Following a similar analysis for a polymerization tank reactor (Gonzalez and Alvarez, 2005), the per-subsystem application of Lyapunov's Converse theorem followed by Gronwall Inequality (LaSalle and Lefschetz, 1961) yields that the CL state and state error motions are bounded as

$$|\boldsymbol{x}(t)| \le s_x(t), |\boldsymbol{x}_E(t)| \le s_E(t) \tag{27a}$$
$$\dot{s}_x = l_z s_x + a_x(l_x^{\tilde{\boldsymbol{\mathit{f}}}} s_e + l_d^{\tilde{\boldsymbol{\mathit{f}}}} \varepsilon_{d_a}), \qquad s_x(0) = s_{xo} \tag{27b}$$
$$\dot{s}_E = l_E s_x + a_E(l_x^{\tilde{\boldsymbol{\mathit{f}}}_E} s_x + l_d^{\tilde{\boldsymbol{\mathit{f}}}_E} \varepsilon_{d_a}), \quad s_E(0) = s_{Eo} \tag{27c}$$

where

$$l_z = \lambda_z - a_x l_x^{\tilde{\boldsymbol{\mathit{f}}}} > 0, \qquad l_E = \lambda_E - a_E l_{\tilde{x}_E}^{\tilde{\boldsymbol{\mathit{f}}}_E} > 0$$

or equivalently

$$|\boldsymbol{x}(t)| \le s_x(t),\ |\boldsymbol{x}_E(t)| \le s_E(t) \quad (28a)$$

$$\dot{\boldsymbol{s}} = \boldsymbol{A}(\omega)\boldsymbol{s} + \boldsymbol{b}\varepsilon_{d_a},\quad \boldsymbol{s}(0) = \boldsymbol{s}_o \quad (28b)$$

where

$$\boldsymbol{s} = \begin{bmatrix} s_x \\ s_E \end{bmatrix},\quad \boldsymbol{A}(\omega) = \begin{bmatrix} l_z & a_x l_{\tilde{x}_E}^{\tilde{f}} \\ a_E l_x^{\tilde{f}_E} & l_E \end{bmatrix},\quad \boldsymbol{b} = \begin{bmatrix} a_x l_d^{\tilde{f}} \\ a_E l_d^{\tilde{f}_E} \end{bmatrix}$$

with $\boldsymbol{A}(\omega)$ Hurwitz if and only if

$$\lambda_E(\omega) >_r a_E l_{\tilde{x}_E}^{\tilde{f}_E} + a_x a_E l_{\tilde{x}_E}^{\tilde{f}} l_x^{\tilde{f}_E}/(\lambda_z - a_x l_x^{\tilde{f}}) := \lambda_D(\omega)$$

or ($\in_r$: robustly inside)

$$\lambda_T(\omega) >_r 0 \ \Leftrightarrow\ \omega \in_r \Omega := [\omega^-, \omega^+] \quad (29)$$

where $\omega^-$and ω^+ are the two roots of the threshold equation

$$\lambda_T(\omega) := \lambda_E(\omega) - \lambda_D(\omega) = 0$$

where the stabilizing (or destabilizing) term λ_E (or λ_D) depends linearly (or linearly and quadratically) on the estimator gain ω. This result is stated next in proposition form.

Proposition 1. The CL system (18) is robustly stable if the estimator gain ω of the G estimator (23a-d) is robustly inside the gain interval Ω (29), i.e.,

$$\omega \in_r \Omega := [\omega^-, \omega^+].\ \bullet \quad (30)$$

The lower limit condition ($\omega >_r \omega^-$) ensures stability with small gain, and the upper one ($\omega <_r \omega^+$) (which corresponds to the ultimate gain in industrial tuning) precludes destabilizing by excessive noise-like high frequency amplification of modeling, measurement and actuator errors.

Following the tuning guidelines of the GE [Alvarez and Fernandez et. al., 2009] and regulation gain (k) [Alvarez et al., 2004; Gonzalez and Alvarez, 2005] in the light of the closed-loop stability considerations of Section 5.1, the OF controller (23) is set with industrial-like guidelines:

$$\zeta \in [1, 4],\quad \omega = n_\omega \lambda_r,\quad n_\omega \in [5, 30] \quad (31a)$$

$$k = n_c \lambda_r,\quad n_c \in [2, 5],\quad \lambda_r\text{: (13)} \quad (31b)$$

followed by simulation and/or plant testing-based gain calibration, with an important addition: the sensor location (23e) of the proposed NL OF controller (23) is determined by structural (with respect to axial position) tuning, starting with the industrial sensitive location (with maximum temperature slope change before the hot spot) for control (Bashir et al., 1992) and estimation (Van den Berg, 2000).

6. FUNCTIONING

In this subsection, the efficient model-based OF-FF control (23) is applied to the gasification reactor example (8).

The application of the tuning guidelines (31), with initial sensor placed at the sensitive location ($l = 1 \Rightarrow z_l = 1.6$ cm), yields

$$\zeta = 3.5,\ n_\omega = 10,\ n_c = 4;\ l = 4\ \Rightarrow\ z_l = 6.5 \text{ cm} \quad (32a\text{-}b)$$

It must be pointed out that the CL system with: (i) the best sensor location $l = 4$ converged to the nominal ignition SS of interest, manifesting ZD is robust monostability, and (ii) for (incorrect) location $l \in [14, 30]$ the CL converged to an extraneous (undesired) ignition attractor, manifesting ZD multistability.

In Fig. 4, the response of the CL reactor temperature profile to the solid flow disturbance (top panel fig. 3) with sensor at $z_l = 6.5$ cm is presented, showing that after a towards-extinction excursion, the controller steers back the reactor to the prescribed ignition SS avoiding the OL extinction (fig. 3).

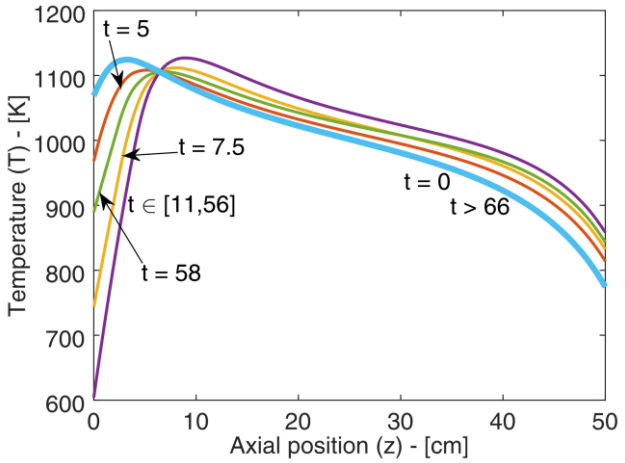

Fig. 4. Closed-loop (CL) responses of the temperature profile to the solid feed flow disturbance (top panel fig. 3) with sensor at $z_l = 6.5$ cm ($l = 4$).

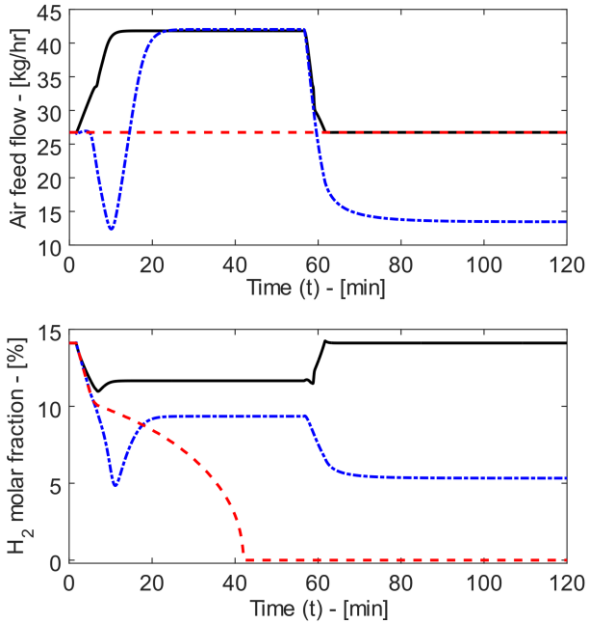

Fig. 5. Open (dashed curve) and closed (black and blue curves)-loop responses of the air feed flow control (top panel) and effluent hydrogen fraction (bottom panel) to the solid feed flow disturbance (fig. 3), for: (i) best location $z_l = 6.5$ ($l = 4$), and (ii) incorrect location 24.2 cm ($l = 15$).

For comparison and illustration purposes, the CL reactor subjected to the solid feed flow disturbance of Fig. 3 was set with the right (or wrong) sensor location $l = 4$ at $z_l = 6.5$ cm (32b) (or $l = 15$ at $z_l = 24.2$ cm), yielding the effluent hydrogen concentration (top panel) and air feed flow rate control action (bottom panel) compared with the OL ignition-

to-extinction SS response. The OL reactor reaches the extinction SS with null hydrogen production, evidencing the need of feedback control. While CL reactor with the right sensor remains at the ignition SS of interest, the CL reactor with the wrong sensor reaches an extraneous ignition SS with 60 % lower nominal hydrogen production. This demonstrates the disturbance rejection capability of the proposed controller, preventing reactor extinction. The 10 concentration-1 temperature-2 flows-state profile estimate quickly converges (in approx. 10 s), with robustness to noise and reasonable parameter error (not shown due to space limit).

7. CONCLUSIONS

The problem of robustly controlling an open loop bistable tubular gasification reactor about its ignition stable SS has been resolved with an efficient model-based OF-FF control with: (i) solvability assessment according to passivity and detectability, (ii) conventional-like tuning, and (iii) sensor location tuning through spatial calibration.

The proposed methodology was applied to a 10 concentration-1 temperature-2 flows biomass stratified gasifier through simulations, yielding an OF-FF made by a 30-stage model-based 90 ODEs and 300 AEs with sensor location at the slope inflection point (one tenth of the reactor length) after the hot spot. The importance of the sensor location was verified: when it is located in the middle of the reactor, the admissible input disturbance reactor reaches an extraneous CL SS with caloric content significantly smaller than the one of the SS of interest.

The present study is a point of departure to: (i) formally characterize, with bifurcation analysis, the passivity and detectability properties, and (ii) improve behavior through incorporation of more sensors and stage number reduction.

REFERENCES

Alvarez, J., Fernandez, C. (2009). Geometric estimation of nonlinear process systems, *Journal of Process Control*, 19, 247–260.

Alvarez J., Zaldo F. and Oaxaca, G. (2004). Towards a Joint Process and Control Design Approach for Batch Processes: Application to Semibatch Polymer Reactors. In *Integration of Process and Control Design*, M. Georgiadis, and S. Panos Eds., Elsevier, 604-634.

Badillo-Hernandez, U., Nájera, I., Álvarez, J. and Alvarez-Icaza, L. (2017). State profile estimation in a biomass gasification tubular reactor. *IFAC-PapersOnLine, 50, 10208-10213*.

Badillo-Hernandez, U., Alvarez, J. & Alvarez-Icaza, L. (2019). Efficient modeling of the nonlinear dynamics of tubular heterogeneous reactors. *Computers & Chemical Engineering,* 123, 389-406.

Bashir, S., Chovln, T., Masri, B. J., Mukherjee A., Pant A., Sen S., and Vijayaraghavan P., (1992). Thermal Runaway Limit of Tubular Reactors, defined at the Inflection Point of the Temperature Profile. Ind. Eng. Chem. Res., 31, 2164-2171.

Beniich, N., El Bouhtouri A. & Dochain, D. (2017) Adaptive local tracking of a temperature profile in tubular reactor with partial measurements, J. Process Control. 50, 29–39.

Di Blasi, C. (2000). Dynamic behavior of stratified downdraft gasifiers. *Chemical Engineering Science*, 55, 2931–2944.

Dixon, R. & Pike, A. W. (2006). Alstom Benchmark Challenge II on Gasifier Control. Control Theory and Applications, IEE Proceedings, 153, 254-261.

Fernandez, C., Alvarez, J., Baratti, R., and Frau, A. (2012). Estimation structure design for staged systems. *Journal of Process Control*, 22 (10), 2038-2056.

Gonzalez, P. and Alvarez, J. (2005). Combined Proportional/Integral-Inventory Control of Solution Homopolymerization Reactors, *Ind. Eng. Chem. Res.*, 44, 7147-7163.

Hlavacek, V. (1970). Aspects in design of packed catalytic reactors. *Industrial & Engineering Chemistry*, 62(7), 826.

Khalil, H.K. (2002). Nonlinear Systems, 3rd ed., Prentice Hall.

La Salle, J., Lefschetz, S. (1961). Stability by Liapunov's Direct Method, Academic Press: New York.

LeVeque, R. J. (2007). Finite difference methods for ordinary and partial differential equations: steady-state and time-dependent problems. *SIAM*, Philadelphia.

Manurung, R., & Beenackers, A. (1993). Modeling and simulation of an open core downdraft moving bed rice husk gasifier. *Advances in Thermochemical Biomass Conversion*, 1, 288–309.

Meurer, T. & Zeitz, M. (2008) Model inversion of boundary controlled parabolic partial differential equations using summability methods, Math. Comput. Model. Dyn. Syst. 14, 213–230.

Nájera, I., Álvarez, J., Baratti, R., Gutiérrez, C. (2016) Control of an exothermic packed-bed tubular reactor, *IFAC-PapersOnLine*, 49, 278-283.

Pérez, J.F., Melgar A. and Benjumea P.N. (2012). Effect of operating and design parameters on the gasification/combustion process of waste biomass in fixed bed downdraft reactors: An experimental study, *Fuel*, 96, 487-496.

Porru, M., Alvarez, J. and Baratti, R. (2013). Composition Estimator Design for Industrial Multicomponent Distillation Column, *Chemical Engineering Transactions*, 32, 1975-1980.

Rogel, A., & Aguillon, J. (2006). The 2d eulerian approach of entrained flow and temperature in a biomass stratified downdraft gasifier. *American Journal of Applied Sciences*, 3, 2068–2075.

Sontag, E.D. (2000). The ISS philosophy as a unifying framework for stability-like behavior, in: A. Isidori, F. Lamnabhi-Lagarrigue, W. Respondek (Eds.), *Nonlinear Control in the Year 2000*, Vol. 2, Springer-Verlag, Berlin, pp. 443–468.

Van den Berg, F.W.J., Hoefsloot, H.C.J., Boelens, H.F.M. & Smilde, A.K. (2000). Selection of optimal sensor position in a tubular reactor using robust degree of observability criteria, Chemical Engineering Science, 55, 827–837.